Three dimensional two point ray tracing using paraxial rays in cartesian coordinates

Ronit Strahilevitz, Paradigm Geophysical; Dan Kosloff, Department of Geophysics, Tel Aviv University, Israel and Paradigm Geophysical; Zvi Koren, Paradigm Geophysical*

Summary

Paraxial rays are used for 3D two point ray tracing in complex structures. In this work we use dynamic ray tracing which is formulated in cartesian coordinates. This formulation allows for more flexibility in perturbing the initial slowness and takeoff point of the rays, as compared to the more common dynamic ray tracing in ray centered coordinates. Furthermore, the paraxial rays are adjusted iteratively to conform to the surface and interface topography, and to have slowness vectors with the correct length. This extends considerably the range of validity of the paraxial approximation. We describe implementation of different types of two point ray tracing which include CRP ray tracing, normal incidence ray tracing and CMP ray tracing.

Introduction

Three dimensional ray tracing in complex structures can be very cumbersome and slow. Two point ray tracing in particular is difficult because of the need to have the rays converge to specified surface locations or to specified offsets. In this work we adopted from Virieux et al (1988) a formulation of dynamic ray tracing in cartesian coordinates for performing two point ray tracing. This formulation has the advantage of working in a single coordinated system instead of having to transform between a local ray centered system and the global system. In addition the cartesian formulation allows for three dimensional perturbations in the initial takeoff point of the ray and the initial slowness, as opposed to the two dimensional perturbations perpendicular to the initial ray which are allowed in ray centered dynamic ray tracing.

We describe implementation of dynamic ray tracing for CRP ray tracing, normal incidence ray tracing and CMP ray tracing. In addition to the original formulation of Virieux et al (1988), in our implementation the paraxial rays are adjusted iteratively to conform to varying surface and reflector topography and velocity, and for possessing a correct magnitude of the initial slowness at the takeoff location.

Basic Equations

The ray equations are given by;

$$\frac{dx_i}{d\sigma} = p_i$$

$$\frac{dp_i}{d\sigma} = u\frac{\partial u}{\partial x_i}$$

$$i = 1.3$$

(Eq. 1)

Where $x_i(\sigma)$ is the ray path, $p_i(\sigma)$ is the ray slowness, $u = 1/c$ with $c(x, y, z)$ the medium velocity, and $\sigma = \int_{ray} c^2 dt$ with t the travel time.

Given a central ray with ray path $x(\sigma)$ and slowness $p(\sigma)$, we consider a neighboring ray with path $x(\sigma) + \delta x(\sigma)$ and $p(\sigma) + \delta p(\sigma)$. It was shown by Virieux et al (1988) that to first order,

$$\delta x = Q_1 \delta p^0 + Q_2 \delta x^0$$

and,

$$\delta p = P_1 \delta p^0 + P_2 \delta x^0$$

where δp^0 and δx^0 are the perturbations in the initial ray slowness and takeoff points respectively. Q_i and P_i are 3 by 3 matrices which satisfy the coupled equations:

$$\frac{dQ_i}{d\sigma} = P_i$$

$$\frac{dP_i}{d\sigma} = \frac{1}{2}\nabla\nabla u^2 Q_i$$

(Eq. 2)

With initial conditions $Q_1(0) = 0$, and $P_1(0) = I$ and $Q_2(0) = I$, $P_2(0) = 0$ with I the unit matrix. In the following we describe the use of these equations for different types of two point ray tracing.

A single ray connecting a subsurface point and a specified point on the surface

Assume that a central ray has been traced from a subsurface point A (Fig. 1) to the surface. This ray hits the surface at point B which is at a distance dx from the target surface point C. Denoting the surface topography by the function $F(x, y, z) = z - f(x, y) = 0$ and denoting δx the distance between the surface termination of central ray and the paraxial ray at point B (Fig. 1), the quantities are related by,

$$dx = \delta x + p(x + \delta x)\tau, \qquad \text{(Eq. 3)}$$

Where $d\tau$ is the remaining travel time along the paraxial ray to the surface (can also be negative). Since δx is not known a priori, $p(x + \delta x)$ is obtained iteratively where δx from the previous iteration is used. A scalar multiplication of (3) by ∇F and use of the orthogonality of ∇F to dx, yields a relation connecting dx and δx;

$$dx = \delta x - \frac{p\delta x}{\nabla F p}$$

(Eq. 4)

(Farra et al, 1989). In the current configuration where $\delta x^0 = 0$, equations (2) and (4) yield a direct connection between the surface distance dx and the initial slowness perturbation δp^0. We expand δp^0 as a linear combination;

$$\delta p^0 = \alpha p^0 + \beta_1 p^1 + \beta_2 p^2$$

(Eq. 5)

where p^1 and p^2 are two coperpendicular vectors which are also perpendicular to the initial slowness p^0. An additional constraint which is imposed on δp^0 is that the perturbed slowness be of the correct magnitude,

$$\left| p^0 + \delta p^0 \right| = u^0$$

(Eq. 6)

The horizontal components of equation (4) together with (2),(5) and (6) constitute a determinate set of equations for the unknowns α , β_1 and β_2 . The system is solved iteratively.

Normal incidence ray tracing

In this case the central ray is normal to the interface from which it emerges and impinges on the surface at a distance dx from the desired location (Fig. 2b). For the paraxial ray we seek a perturbation δx^0 parallel to the interface from which the ray emerged. However when the interface is not flat, there is also a change δp^0 in initial slowness. Consequently, δx^0 and δp^0 are calculated iteratively.

CRP ray tracing

In this ray tracing the objective is to find a ray pair which obeys Snell's law at the initial point and reaches the surface at a specified vector offset $2h$ (Fig. 2c). First a central ray pair satisfying Snell's law is traced. Denoting δh the difference between the desired half offset and the actual offset of the central ray pair, the two respective rays are perturbed by respective amounts δp_1^0 and δp_2^0 . The perturbed rays reach the surface at the specified offset and obey Snell's law at their point of emergence.

CMP ray tracing

CMP ray tracing (Fig. 2d) is affected by first shooting a ray pair which obeys Snell's law. Denoting dx_1 and dx_2 the distances between the ray pair and the shot and receiver positions respectively, we seek perturbations $\delta {p_1}^0$, $\delta {p_2}^0$ and δx^0 for which the paraxial ray pair will reach the respective shot and receiver locations and will also obey Snell's law at the point of emergence.

Example

We illustrate the paraxial ray tracing for perturbation of single rays connecting a subsurface point and specified surface locations. The example is of a complex 3D structure consisting of layers with laterally varying velocity. Fig. 3 depicts a section of the velocity model. The 3D paraxial ray tracing is tested for a line which is at an angle to the dip direction of the structure. For the tests, a fan of rays originating from the spatial location $x_0 = 2000m$, $y_0 = 2000m$, and $z_0 = 2000m$ with respective takeoff angles of $0 = 20.28^0$ $\phi = -30 + (i-1) \cdot d\phi$, $d\phi = 60/9$, $i = 1,10$, was traced. Next we calculate paraxial rays to predict one traced ray from the previous traced ray. Fig. 4 presents a comparison between the exact rays (solid lines) and the paraxial rays (dots). It can be observed that the real rays and the paraxial rays are virtually indistinguishable. The corresponding travel times of the two types of rays are compared in Table 1. The table shows that the accuracy is greater than one sample, in spite of the fact that the extrapolated distances of the paraxial rays, dx , were around 160m.

Conclusions

We have presented a methodology for three dimensional two point ray tracing based on paraxial rays in cartesian coordinates. This procedure is both accurate and computationally fast. Use of a cartesian formulation instead of the more common ray centered coordinates formulation allows more degrees of freedom for the perturbations. Furthermore, adding nonlinearity to account for varying surface and reflector topography and for normalizing the magnitude of the perturbed slowness extends considerably the range of validity of the approximation.

References

Farra, V., Virieux, J., and Madariaga, R., 1989. Ray perturbation for interfaces. Geophys. J. Int. 99, p377-390.

Virieux, J., Farra, V., and Madariaga, R., 1988. Ray tracing for earthquake location in laterally heterogeneous media. JGR Vol 93, No b6, p6585-6599.

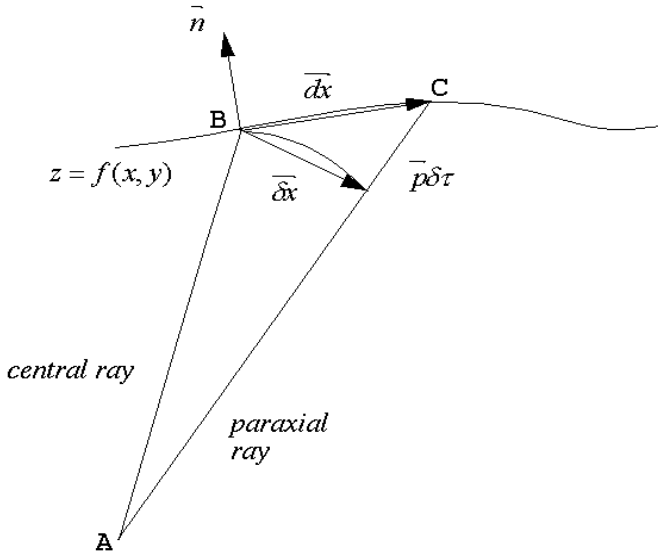

Fig. 1: Single ray configuration

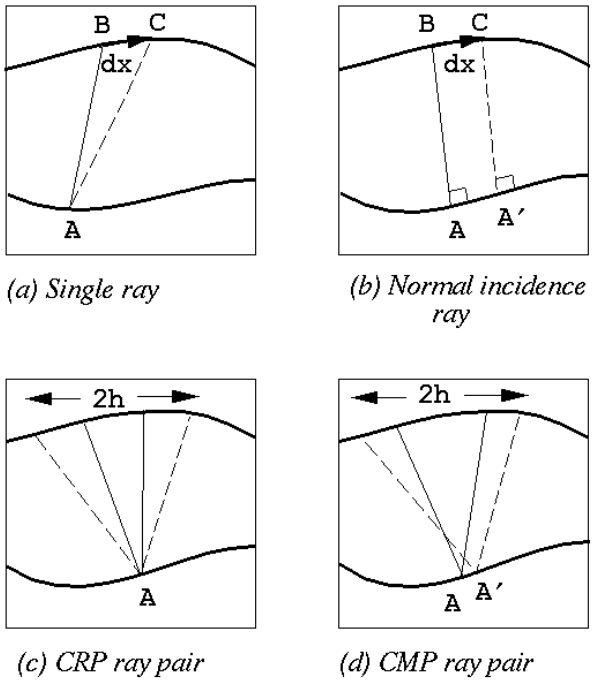

Fig. 2: Shooting configurations

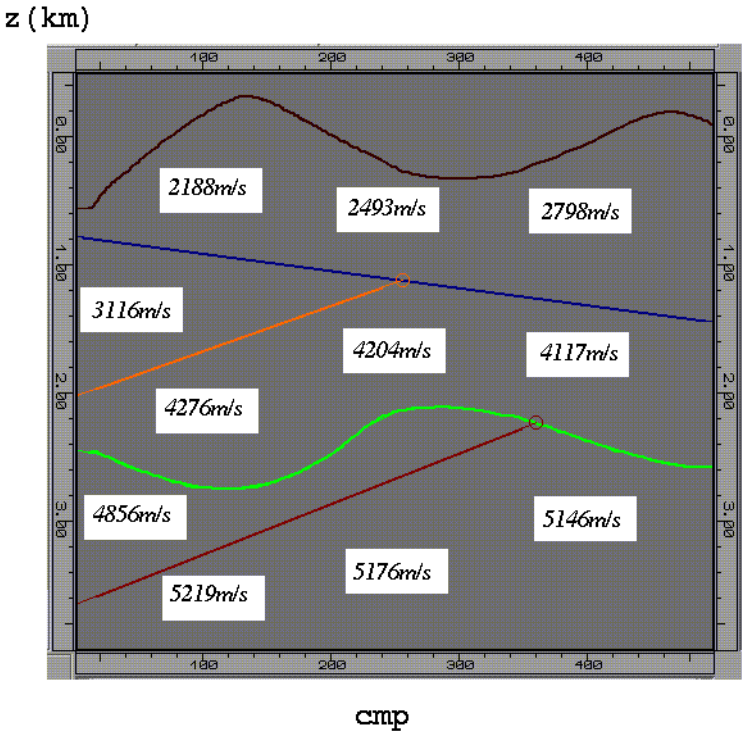

Fig. 3: Section of the subsurface model

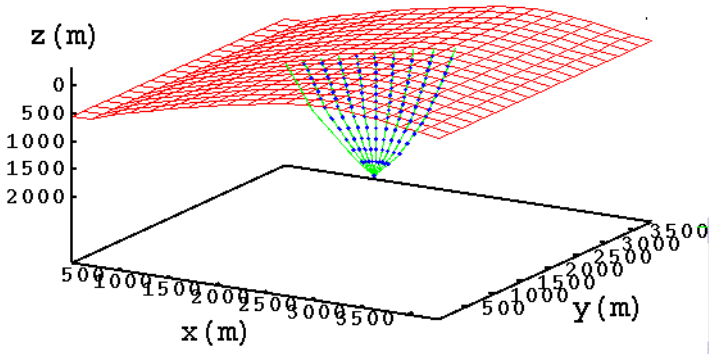

Fig. 4: A comparison between the real rays (solid lines) and the paraxial rays (dots)

ray	dx [m]	dy [m]	ray time [sec]	paraxial time [sec]
1	149.08	54.48	0.7650	0.7648
2	150.83	55.42	0.7704	0.7704
3	150.08	55.96	0.7826	0.7826
4	153.05	57.74	0.7959	0.7959
5	156.89	58.03	0.8125	0.8124
6	161.46	61.87	0.8337	0.8337
7	167.41	63.38	0.8551	0.8549
8	174.19	66.92	0.8799	0.8797
9	177.35	68.21	0.8973	0.8968

Table 1: Traveltime comparision of the real and paraxial rays